

Field-Scale Model for Air Sparging Performance Assessment and Design

G. Hein (email: glhein@mtu.edu)

N. Hutzler (email: hutzler@mtu.edu)

J. Gierke (email: jsgierke@mtu.edu)

**Department of Civil and Environmental Engineering
and**

Department of Geological Engineering and Sciences

Michigan Technological University

1400 Townsend Drive

Houghton, MI 49931-1295

R. Falta (faltar@clemson.edu)

Department of Earth Sciences

Brackett Hall, Box 341906

Clemson University

Clemson, SC 29634-1908

**Research Sponsored by U.S. Department of Energy's Morgantown Energy Technology
Center, under Contract Number: DE-RO21-95MC33082 with Michigan Technological
University, 1400 Townsend Drive, Houghton, MI 49931-1295, telefax: (906) 487-3371
Contract Manager: Karl Frohne**

Disclaimer

This report was prepared as an account of work sponsored by an agency of the United States Government. Neither the United States Government nor any agency thereof, nor any of their employees, makes any warranty, express or implied, or assumes any legal liability or responsibility for the accuracy, completeness, or usefulness of any information, apparatus, product, or process disclosed, or represents that its use would not infringe privately owned rights. Reference herein to any specific commercial product, process, or service by trade name, trademark, manufacturer, or otherwise does not necessarily constitute or imply its endorsement, recommendation, or favoring by the United States Government or any agency thereof. The views and opinions of authors expressed herein do not necessarily state or reflect those of the United States Government or any agency thereof.

Introduction

Air sparging has been used as an *in situ* technique to remove VOCs from contaminated groundwater. Very few studies have been completed to quantify the remediation regime or the mass transfer processes. Figure 1 shows a typical air sparging field installation.

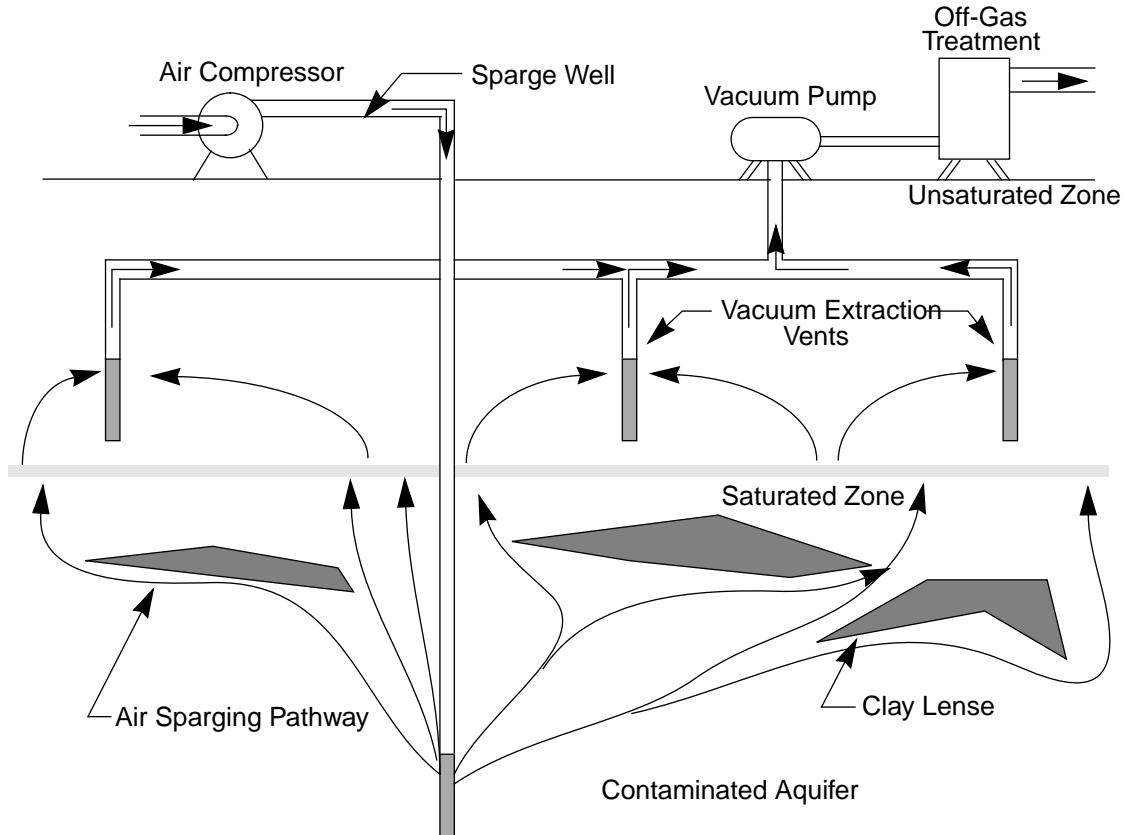


Figure 1: Air Sparging Field Schematic

As shown in this figure, air is injected into the groundwater from an injection well. The VOC partitions into the air phase and rises to the unsaturated zone. At this point, another technology, typically soil vapor extraction (SVE) is used to remove the gases from the vadose zone.

Problem

Existing methods used to estimate the effectiveness of air sparging and the time required for treatment are unrealistic because the flow and mass transfer processes are not well understood. Many existing models do not consider mass transfer processes or they define the air flow patterns insufficiently. Therefore, the time required for a site clean-up is under estimated, while the air sparging regime is over-predicted. A computer model that more accurately describes this process is needed.

Solution

A logical sequence of experiments will be performed to identify the mechanisms controlling mass removal and quantify their rates based on basic porous media and chemical properties and hydraulic characteristics. Modeling will be coupled to the experiments to understand the experimental results and to demonstrate the correct mechanistic approach that will be used in developing a field-scale performance assessment model. The field-scale performance assessment model will be tested against field data obtained under controlled conditions.

Project Description

To complement ongoing field and laboratory research into air flow patterns induced by air sparging, there is a critical need to perform controlled laboratory experiments to identify and quantify mass transfer rates for air sparging. The mass transfer study will be performed in such a manner that it can be incorporated into existing theoretical frameworks for air flow patterns and can be used for design guidance. Controlled experiments are needed because the important processes are not well understood nor even positively identified. The research study of mass transfer will include a demonstration of the appropriate approach to model mass transfer. A theoretical model will also be used to help understand the laboratory results. A field-scale air sparging model is being developed to include mass transfer from the liquid phase to the gaseous phase so that it can simulate the removal of a VOC mixture composed of up to 10 components. The model output will show the extent of remediation, the air pressure distribution and saturation distribution. This information can be used to more accurately design an air sparging system or determine if air sparging is applicable under a given set of conditions.

To test the model, a series of column experiments will be completed for three cases: single-solute, multi-solute and single-NAPL column experiments. The successful completion of the laboratory results will be established by comparing model predictions to the results. Two chemicals (trichloroethylene and toluene) will be used in the experiments. At least five experiments will be performed with each (2 single-solute, 2 multi-solute, and NAPL phase).

The single-solute experiments will be repeated for the following conditions: two different grain sizes and a distribution of grain sizes. The gaseous-phase emissions will be monitored, and the contaminant mass removed will be compared to the amount injected into the column. A residual amount of contaminant should remain in the column. Multi-solute experiments will be completed to see if there are concentration effects. The multi-solute experiments will consist of a two-component mixture of TCE and toluene. Some preliminary column experiments and modeling have been completed. They are outlined in the following section.

The procedures for the single-NAPL experiments will be identical to dissolved solute experiments. A residual saturation of TCE and toluene will be used in these experiments. The residual will be located in the upper portion of the saturated soil column. Tests will be repeated for several residual levels to determine if the mass transfer rate is a function of the amount of residual.

The final test of the model will involve comparing numerical results to field data generated during a pilot-scale air sparging/soil vapor extraction test. The field-scale tests are being performed under a separate award from the EPA. The tests are being conducted in 3x5x10-m deep

cell at Hill AFB, Utah. The soil at Hill AFB is typical of most current sparging applications in that it has a high permeability. The primary contamination is jet fuel (JP-4) so the fullest capabilities of the model will be tested. The test cell is fully instrumented for pressure and concentration monitoring, so there will be comprehensive data sets for model testing. Multiple test conditions will be performed so there will be more than one set of test results for model comparison.

After model testing has been completed, a users' manual will be written such that engineers can use the model to design air sparging systems. The model will be useful to examine performance by varying the location of sparging and vapor extraction wells. Therefore, the time for the VOC to be removed can be determined for a given site configuration and can be compared to other system layouts.

The tasks are outlined in the Figure 2. This flowchart shows how the tasks are related and the order in which they must be performed. As this figure shows, both the experimental work and the modeling are interrelated. For instance, the single solute experiments must compare well to the model predictions before the multi-solute tests and modeling can be completed. Although the flowchart also shows that Michigan Tech and Clemson will be completing designated tasks, the two universities will be working closely together to coordinate and complete the laboratory and numerical experiments.

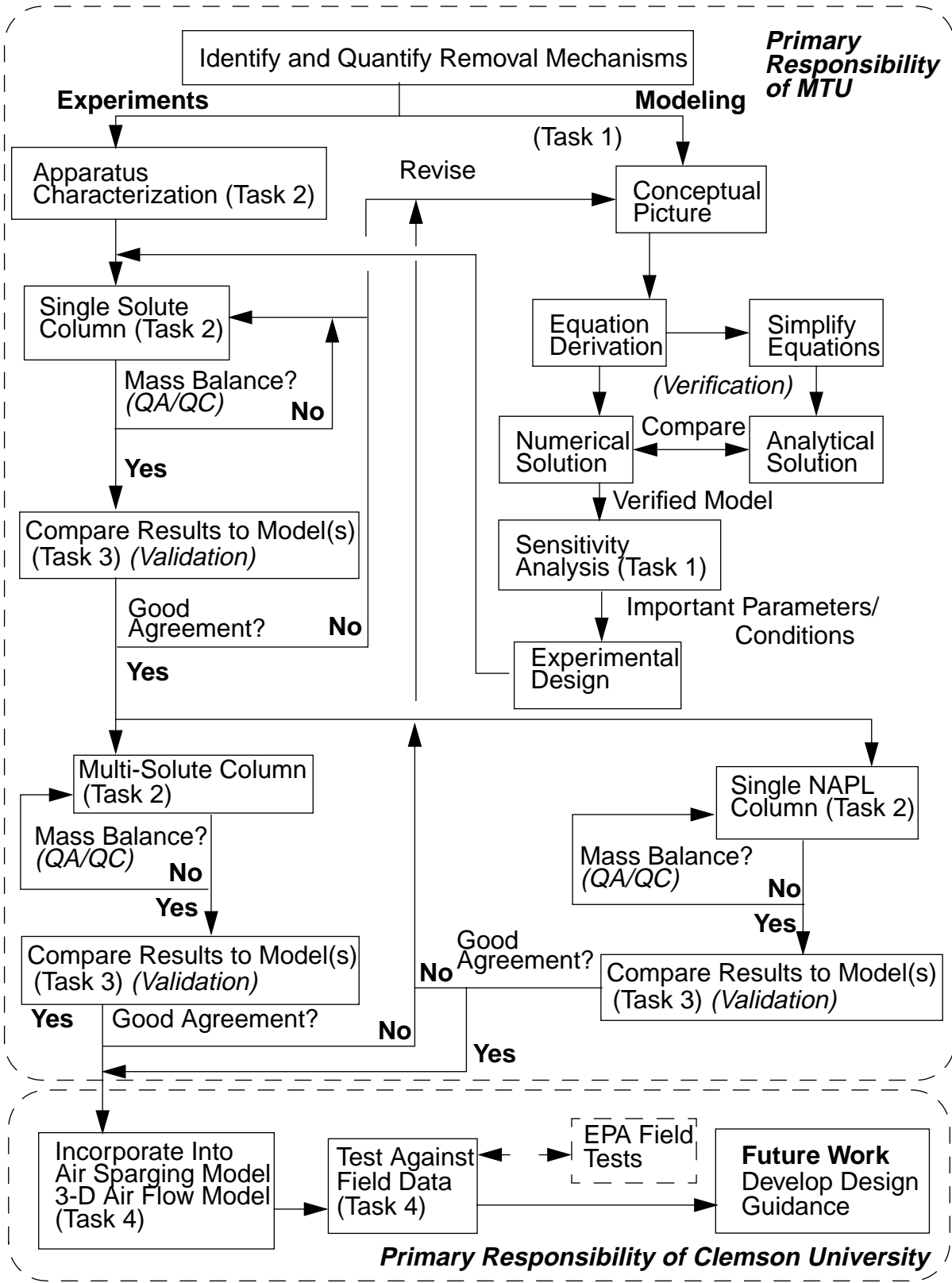


Figure 2: Project Flowchart

Results

Since this project has recently begun, there are only preliminary results available. Preliminary laboratory column tests have been conducted along with some modeling to simulate the removal of a single VOC from a soil column. The comparison of the soil column data and the numerical simulations show that a finite element code is able to predict the removal of methane, a conservative tracer, and TCE, a common VOC in contaminated groundwater. To determine if the air flow pattern generated during air sparging is predictable, experiments were completed in a large-scale reactor and compared to numerical simulations using another numerical model. The description of the experimental conditions and results are included in this section. The column tests are described first followed by the large-reactor experiments.

Soil Column Experimental Apparatus

The soil column experiments were conducted to determine the rate of VOC removal during air sparging. Each experiment was run in duplicate at an injection flowrate of 10 mL/min in a 5.0-cm diameter column containing Ottawa sand according to the schematic shown in Figure 3. Prior to the test, the column was uniformly packed in 0.5 cm lifts with 20 x 30 mesh Ottawa sand to a depth of 14.34-cm. The empty column mass and the mass of the column packed with dry sand were measured to calculate the bulk density and porosity. The column was saturated by recirculating water through it overnight. Once again, the column was weighed to obtain the saturated soil mass. For the next 24 hours, nitrogen was injected through the bottom of the column to displace water and establish air channels. The flow was regulated using a micrometer valve (Swagelock M/N SS-21RS4, Appleton, Wisconsin). The flowrate was measured using a bubble meter (0 to 100 mL, Ace Glass, Vineland, New Jersey) located downstream of the soil column. The displaced water was collected in a beaker to check the degree of saturation. Afterwards, a nitrogen/methane mixture followed by a nitrogen/TCE mixture were fed through the column and to a gas chromatograph (GC) equipped with a thermal conductivity detector (TCD) (MTI M/N 200, Fremont, California) to measure the gaseous-phase concentration. The methane and TCE concentrations in the compressed gas cylinders were both 1000 ppm_v, respectively (Matheson, Chicago, Illinois). Once the chemical concentration in the column effluent became constant, nitrogen was fed through the reactor to sparge the methane or TCE. The process was completed when the normalized concentration dropped to below the detection limit, which is approximately 10 ppm_v. The column was weighed after sparging to calculate the water saturation of the sand. After the test, the mass of water displaced was compared to the difference between the saturated column mass and the column mass after sparging. The difference between the two masses was less than 10 percent.

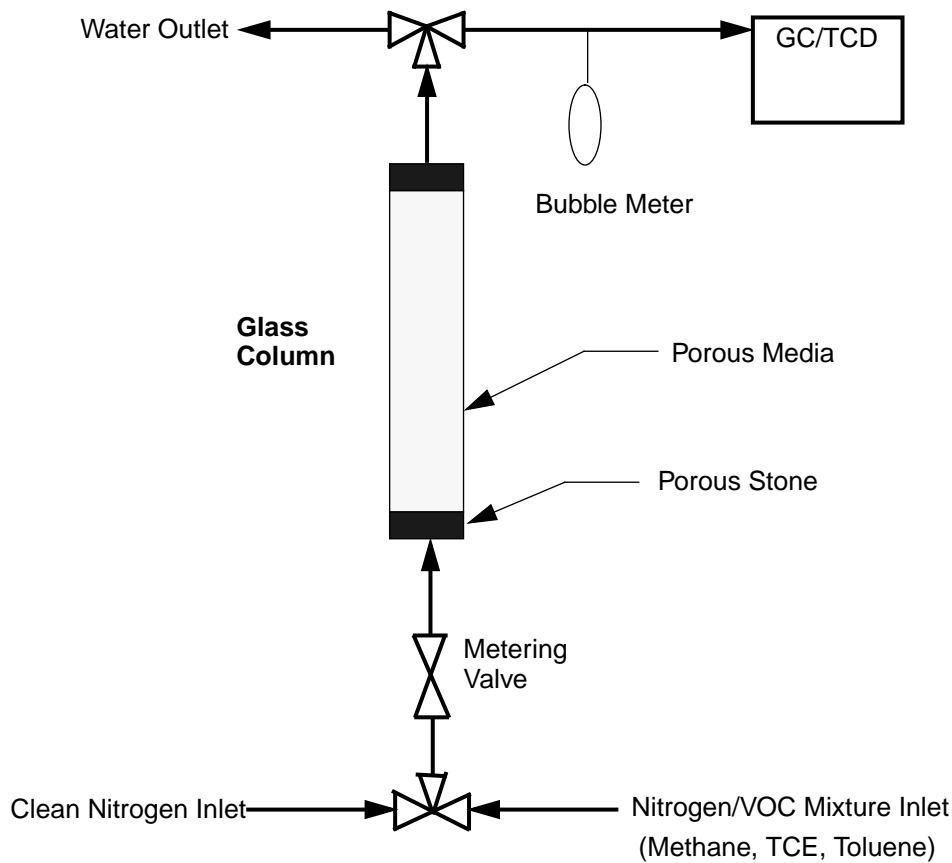


Figure 3: Diagram of Column Tests

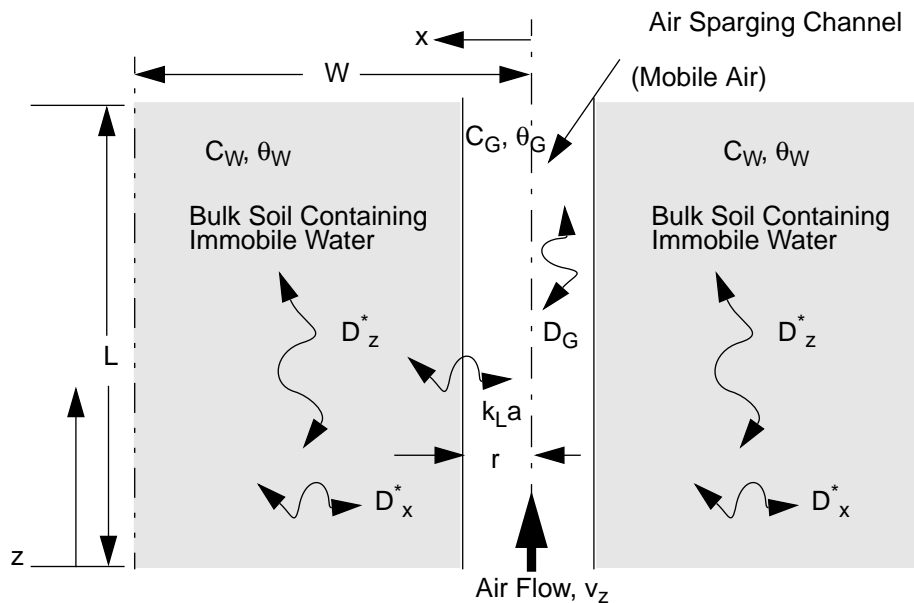
Column Model Development

The model development is based on a sparging system containing an initial VOC concentration and consisting of many equally-spaced channels of uniform size. The concept that air travels in distinct channels is based upon the laboratory work completed by Ji, et al. (1993). They showed that, for fine glass beads, air flowpaths were formed during sparging. Once the system achieved steady-state, the paths were stable. This research hypothesized that the air sparging system could be modeled using a single channel and its associated sparging regime to predict chemical removal. This conceptual picture of air sparging is very similar to the description of fingered flow (Wojick, 1995). Both involve the formation of a mobile region surrounded by an immobile zone. Consequently, a solute transport fingered flow code (SOLTFF, Johnstone, 1995) was modified for air sparging.

SOLTFF is designed to model contaminant transport through fingers of water in soil using a two-dimensional geometry. The preferential paths created by the water fingers causes downward chemical transport. The code uses a finite element technique to solve for chemical concentrations in a stationary bulk fluid phase and a finger containing mobile water. Advection and dispersion occur in the mobile zone, and transverse and longitudinal diffusion control transport in the

immobile region. Dispersion across the immobile/mobile boundary is used to describe the mass transfer between the two regions. SOLTFF also has the capability to simulate the effects of sorption, but this feature was not used in the sparging simulations reported here (Johnstone, 1995). Model verification was completed by Johnstone (1995).

Figure 4 conceptualizes the air sparging channel and the surrounding soil. Although in actuality, the air channel and its associated regime is cylindrical, the system is modeled using two-dimensional rectangular coordinates. Equations were modified to simulate chemical extraction by completing mass balances on the liquid and gaseous phases, applying initial and boundary conditions, and incorporating mass transfer and equilibrium expressions. Then they were converted to dimensionless form to decrease the number of parameters. An overall mass transfer coefficient is included in air sparging equations to account for mass transfer between gas and water. Also, Henry's law is used to describe the equilibrium relationship between the gaseous- and liquid-phase concentrations.



Note: C_W = immobile water phase concentration, C_G = mobile gas phase concentration, θ_W = specific immobile water content based on immobile water volume, θ_G = specific mobile content based on mobile volume, D_z^* = effective liquid diffusion coefficient in the z-direction, D_x^* = effective liquid diffusion coefficient in the x-direction, $k_L a$ = overall mass transfer coefficient between mobile air phase and immobile water phase

Figure 4: Conceptual Picture for the Air Sparging Equation Development

For the air sparging model development, the porous media profile is assumed homogeneous and isotropic. Since the time required for the groundwater to be displaced from the air channel is small compared to the period for remediation, the air channel is present at the initiation of sparging. Air flow is parallel to the z-coordinate and originates from the sparger where the z-coordinate follows the centerline of the sparging channel. The air flow velocity is constant within the sparging channel. This assumption requires that air is treated as an incompressible fluid. In actuality, the air mass flowrate is constant with either the sparging

channel area or the velocity changing with depth. Previous work by Hein, et al. (1994) has shown that the changing cross-sectional area of the sparging channel does not affect the predicted rate of chemical removal. The effect of a variable channel area is negligible because the immobile fluid region is much larger than the air sparging channel. The sparging channel consists of porous media particles, adsorbed water, and air. The width of the sparging area is on the pore scale (Ji, et al., 1993). In the air channel, instantaneous mass transfer is assumed to occur between the sorbed water and the air. Therefore, the pore space is assumed to be completely filled with air. Sorption is also included in the equation development but was not tested in the simulations.

The air-phase mass balance was obtained by completing a mass balance bounded in the x-direction by 1/2 the width of the channel (r) and an incremental length in the z-direction. The accumulation in the air phase equals the amount of mass transferred to the air phase by dispersion, advection, and mass transfer.

The liquid mass balance was completed at the line of symmetry separating two adjacent zones and the outer boundary of the mobile channel ($(W-r)$ on Figure 4). The media in the interfinger region was assumed to be fully saturated with water. The reduction of chemical accumulation in the liquid equals the net mass transport out due to liquid diffusion in the x- and z-directions. Advective transport in the liquid phase is negligible because the flow of groundwater is much slower than the air flow. Like the mobile region, retardation in the interfinger was included in the equation development but was not used in the numerical simulations.

The initial conditions assume that the entering air is clean and that the contaminant in the surrounding porous media is at an initial concentration less than or equal to the contaminant's solubility. The first boundary condition assumes a zero concentration gradient. For the air-phase, the Type II boundary condition is located at the upper boundary of the saturated zone. The liquid-phase zero gradient boundary occurs at the line of symmetry between two adjacent sparging regimes (W). Because the air entering the sparging channel is clean, the second boundary condition for the air phase states that concentration gradient at the inlet is a function of the concentration at that point. The fingered flow boundary condition is different at this location because the water entering the water finger is contaminated. The second boundary condition for the liquid phase is a flux balance at the air/water interface.

To ensure that SOLTFF was adapted properly to air sparging, Henry's constant (H) was set to 1.0 in the air sparging adaptation. Simulations were completed using both numerical models. The outputs from the two simulations were within 1 percent of each other. Therefore, the sparging model was used to simulate the laboratory column tests.

SOLTFF Model Calibration

The results of sparging methane from a 5-cm column were used to calibrate tortuosity for gaseous dispersion in the SOLTFF input file. The removal of methane during air sparging is shown in Figure 5 with the open circles and triangles denoting the first and second tests, respectively. The average retardation coefficient and its standard deviation for the breakthrough and elution of methane were 1.05 and 1.02, respectively (Table 1). For a water saturation of 11 percent and a dimensionless Henry's constant of 26, a retardation of 1.01 was calculated. The 4

percent difference between the theoretical and experimental retardations is within the experimental error of this system.

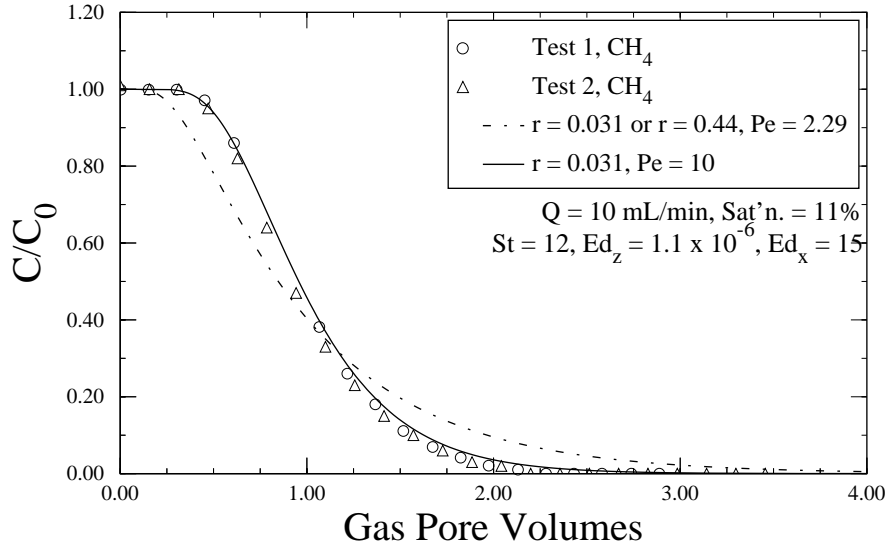


Figure 5: Laboratory Column Data and Numerical Simulations for the Removal of Methane during Air Sparging

Table 1: Experimental, Calculated and Predicted Retardations for the Residual Saturation Sparging Tests ($S_w = 0.11$)

Chem.	Test	Center of Mass		Calc. Retardation ^a $1 + \frac{S_w}{(1 - S_w)H}$	Predicted Center of Mass ^b	Gas Pore Volumes for Gas Injection	Gas Pore Volumes for Test
		Break-through ^b	Elution ^c				
Methane	1	1.06	1.07	1.01	0.99	5.39	7.59
	2	1.03	1.03			5.13	7.59
TCE	1	1.69	1.77	1.35	1.40	10.82	29.92
	2	1.46	1.53			10.77	26.40

- a. S_w = water saturation; H = dimensionless Henry's Law constant
- b. Area obtained from integrating above the curve
- c. Area obtained from integrating under the curve

To calibrate SOLTFF to the methane data, a series of simulations were performed. First, the half-width of the sparging regime (W) was assumed to be approximately 0.035 cm. This dimension was selected because it is approximately one half the width of a sand grain for the silica sand used in these tests. The values for W , θ_w and θ_T were substituted into Equation (1) to solve for the initial channel width:

$$\frac{r}{W} = \frac{\theta_w - \theta_T}{\theta_w} \quad (1)$$

Where r = half of the channel width, W = width between channel and interfinger center lines, θ_w = specific immobile water content based on immobile water volume, and θ_T = total system water content. The ratio, $r:W$, is constant because θ_T and θ_w are constant for a given average water saturation and the model assumptions.

The first methane simulation (dash-dotted line) used the parameters listed in the first column of Table 2. The gaseous diffusion coefficient was adjusted for tortuosity using the Millington and Quirk equation (1961). Based on Henry's law, only 4 percent of the mass of methane entered the gaseous phase. Therefore, altering the channel width did not change the shape of the elution prediction in Figure 5. To see if the effects of gaseous dispersion were due to mechanical mixing or diffusion, the gaseous dispersion coefficient was adjusted until the simulation matched the experimental data. The adjusted curve is shown by the solid line in Figure 5. The fit tortuosity was 6.53 and Pe increased from 2.29 to 10.

Table 2: Model Input Parameters For Toluene and TCE in Ottawa Sand Column

Description	Methane		TCE		Source
	Initial	Fit	Initial	Fit	
Order of Simulations	1		2		Not Applicable
Column Length (cm)	14.34		14.34		Measured
Column Diameter (cm)	5.0		5.0		
Water Saturation, S_w	11%		11%		
Porosity	0.35		0.35		
Air Channel Inj. Vel. per Unit Column Area (cm/min)	0.51		0.51		Calculated
Average Vol. Water Content, θ_T	0.0385		0.0385		
Immobile Vol. Water Content, θ_w	0.35		0.35		
Mobile Vol. Air Content, θ_G	0.35		0.35		From SOLTFF, Air Sparging Equation Development
Gaseous-Phase Tortuosity, τ^a	1.9	6.53	6.53	2.4	Millington and Quirk (1961)
Half Width of Air Channel, r (cm)	0.031		0.031	0.30	Assumed, Pore Scale
Width of Regime, W (cm)	0.035		0.035	0.34	Equation (1)
Channel Half Width: Radius of Regime, $r:W$	1.13		1.13		
Henry's Constant	26		0.35		Hokanson(1996)
Mass Transfer Coef. (s^{-1})	0.2		0.2		Assumed
Aqueous Diff. Coef, D_x (cm^2/s)	9.4×10^{-6}		9.4×10^{-6}	1.7×10^{-7}	Gierke, et al. (1990 and 1992)
Aqueous Diff. Coef, D_z (cm^2/s)	9.4×10^{-6}		9.4×10^{-6}		Gierke, et al. (1990 and 1992)
Gaseous Disp. Coef., D_G (cm^2/s)	1.3×10^{-1}	3.8×10^{-1}	1.4×10^{-2}	3.4×10^{-2}	Gierke, et al. (1990 and 1992)

a. Used to correct gaseous dispersion effects of tortuosity

TCE Column Tests and Numerical Predictions

When TCE was sparged from the soil column, the removal behavior was not as ideal as the data for methane. As shown in Figure 6, Test 1 required more gas pore volumes to remove TCE than Test 2. Test 2, though, had some anomalous readings at the beginning of elution. The differences between the two tests is probably due to experimental error. The two runs required about 10.8 pore volumes to obtain the maximum concentration which is roughly twice the number required for methane. The two tests were stopped after less than 30 gas pore volumes were displaced for breakthrough and elution. After about 4 gas pore volumes were displaced during elution, the normalized concentration reached a minimum value. The average center of mass for breakthrough and elution on the two tests was 1.61 gas pore volumes that resulted in an experimental retardation of 1.51. The calculated retardation for $H = 0.35$ and $S_W = 0.11$ was 1.35. Therefore, a 13 percent difference occurred. Most of the discrepancy could be due to tailing shown in the elution data for TCE as shown in Figure 6.

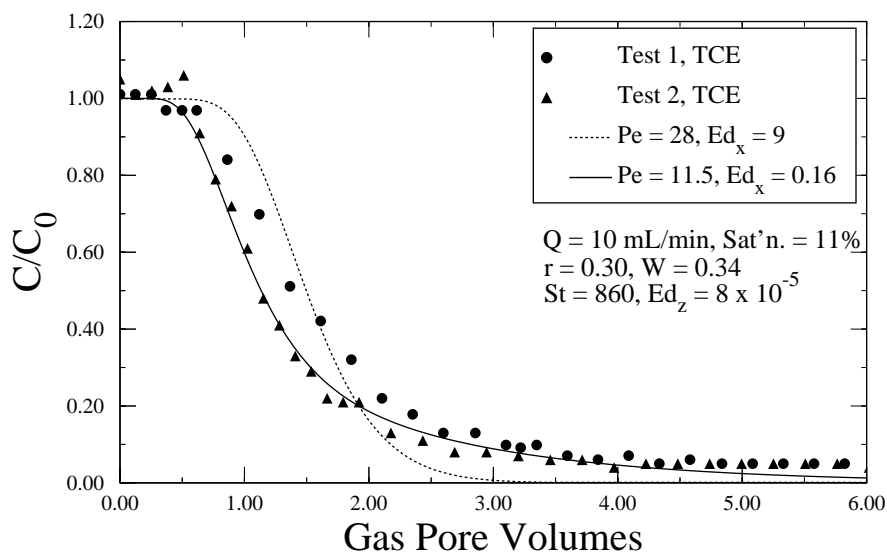


Figure 6: Laboratory Column Data and Numerical Simulations for the Removal of TCE during Air Sparging

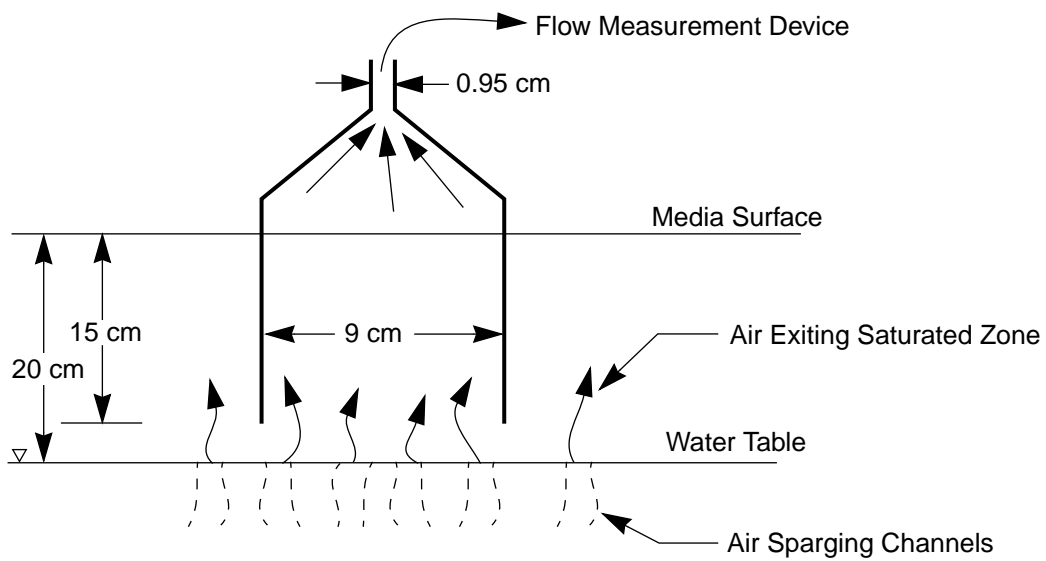
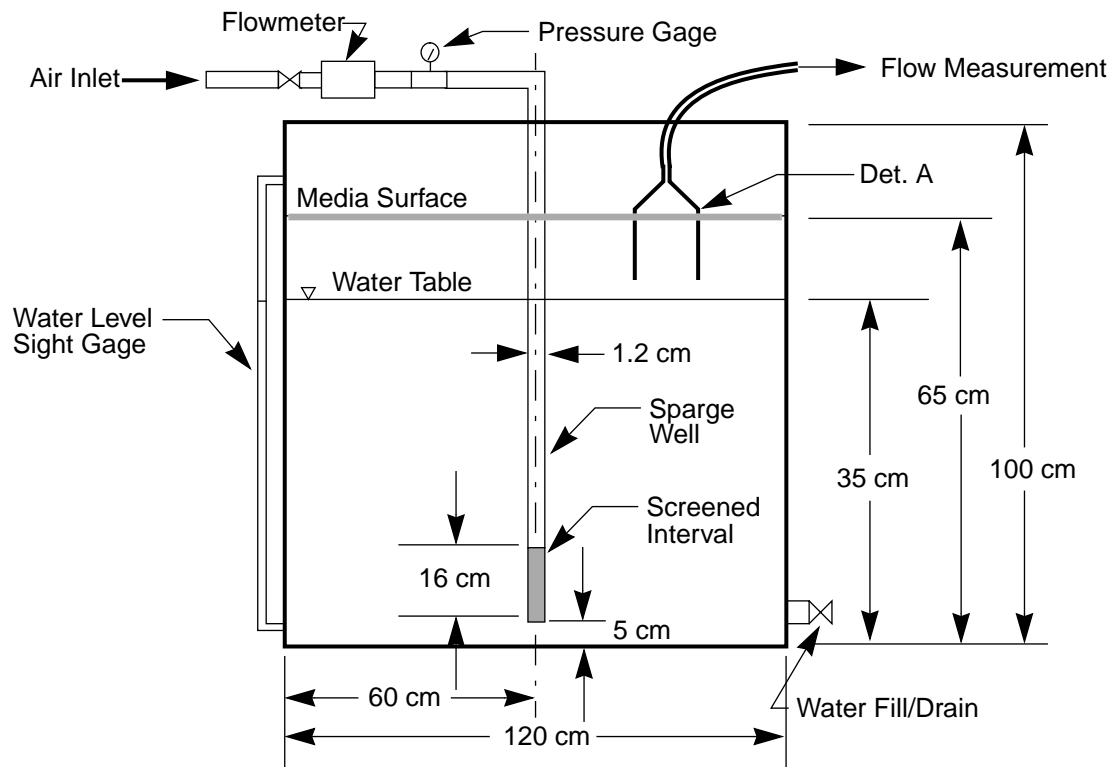
SOLTFE was used to simulate the removal of TCE from the 5 cm dia column where only the gaseous dispersion coefficient was adjusted using the fit tortuosity from the methane prediction. The dashed line in Figure 6 shows the model prediction for $r = 0.30$ cm and $W = 0.34$ cm. This simulation used the values in the “Initial” column in Table 2 where the effective gaseous dispersion coefficient was corrected for a tortuosity of 53. Since the prediction and the data did not match, Pe was decreased from 28 to 11.5. Also, the aqueous diffusion coefficient was reduced to 1.7×10^{-7} cm^2/s . With these parameters, the model simulation matched the data almost exactly. For TCE, the fit gaseous dispersion was greater than the initial, which implies more mechanical mixing in the air channel.

This series of experiments and numerical simulations showed that TCE removal can be simulated through the modification of a solute transport fingered flow code. The predictions

showed the importance of liquid diffusion during air sparging. These experiments also showed that additional work is needed to show how VOC removal is affected under more complex conditions.

Preliminary Large-Scale Reactor Experiments

These simulations will utilize another numerical model, T2VOC (Falta, *et. al.*, 1995). To gain knowledge of the air flow and water behavior around air injection wells, preliminary laboratory tests and model simulations were completed at three injection flow rates (62, 187, and 283 LPM) in a cylindrical reactor (diameter = 1.2 m, depth = 0.65 m) (Figure 7). Measurements of the air flux distribution were made across the surface of the reactor at 24 monitoring locations, 6 radial positions equally spaced along 2 orthogonal transects (Figure 8). Simulations using a multiphase flow model called T2VOC were completed for a homogeneous, axi-symmetric configuration. Input parameters were independently measured soil properties. In all the experiments, about 75 percent of the flow injected exited the water table within 30 cm of the sparge well. Predictions with T2VOC showed the same. The averages of 4 flux measurements at a particular distance from the sparge well compare satisfactorily with T2VOC predictions. Measured flux values at a given radius varied by more than a factor of 2, but the averages were consistent between experiments and agreed well with T2VOC simulations. The T2VOC prediction of the radial extent of sparging coincided with the distance out to which air flow from the sparge well could not be detected in the reactor. The sparging pattern was relatively unaffected by the air injection rate over the range of conditions studied. Changes in the injection rate resulted in nearly proportional changes in flux rates.



Detail A: Flow Measurement Device
Figure 7: Cross-Sectional View of the Vessel Used to Measure Air Fluxes Emerging from the Water Table during Air Sparging

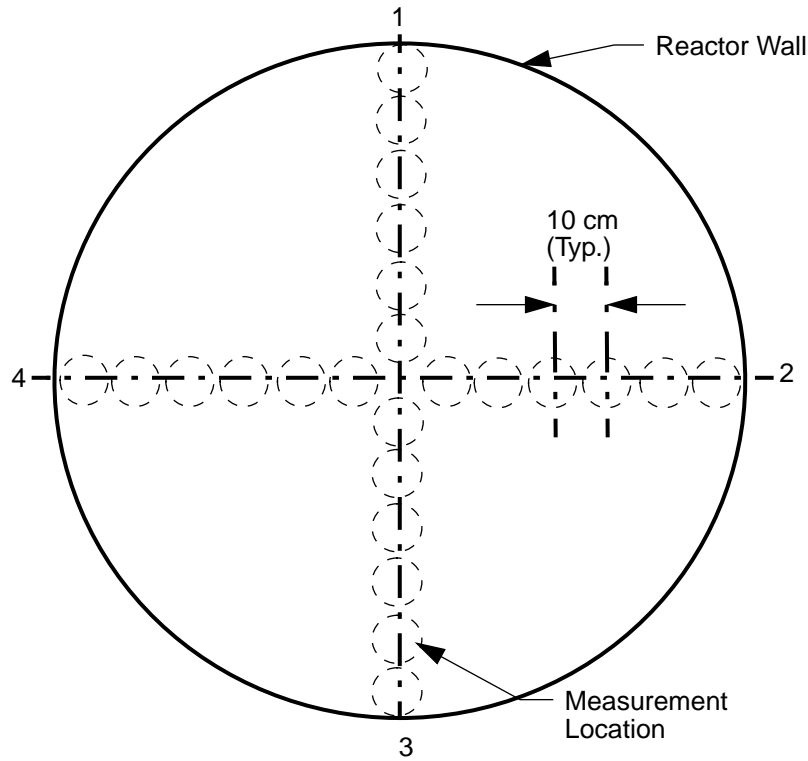


Figure 8: Plan View of Sparging Vessel Showing Measurement Locations

T2VOC Model Description and Simulation Configuration

The numerical simulations using T2VOC were completed for an isothermal, axisymmetric, homogeneous, isotropic system under two-phase (air and water) flow conditions. The model assumes air and water flow are described by Darcy's Law extended to multiphase systems. Air and water saturations, pressures, and permeabilities are related through empirical functions (pressure-saturation and saturation-permeability) as denoted below.

Accurately modeling the air fluxes and saturations is particularly important for air sparging simulations because they impact the removal rate and region of influence. Higher air saturations result in better contact with the contaminated water phase or the NAPL phase, resulting in greater volatilization of the contaminant. If adequate contact does not occur, the chemical will not readily partition into the air phase (Unger et al., 1995).

The air saturation is governed by the soil's wetting (capillary) characteristics. A common relationship used to describe a soil moisture characteristics (pressure versus saturation) is an equation presented by van Genuchten (1980):

$$P = \frac{\rho_w g}{\alpha} \left[\left(\frac{S_w - S_{wr}}{1 - S_{wr}} \right)^{\frac{n}{1-n}} - 1 \right]^{\frac{1}{n}} \quad (2)$$

where: P = water pressure (Pa), ρ_w = water density (kg/m^3), g = gravitational acceleration (m/s^2), S_w = water saturation, S_{wr} = irreducible water saturation, and α (m^{-1}) and n (dimensionless) are empirical constants fit to measured P vs. S_w data.

Equation (10) is used in T2VOC to describe the capillary effects. To obtain the fitted parameters (α , n), the van Genuchten equation (1980) was fit to pressure versus water saturation data using a program (Megafit) developed by Parker et al. (1987). The value of S_{wr} was assumed to be the water saturation at 500 cm of suction. The pressure-saturation data were obtained from an independent laboratory analysis (Daniel B. Stephens and Associates, Inc., Albuquerque, New Mexico) of a 270-g sand sample. The measured data are shown in Figure 9 along with the calibration of equation (10). Table 3 lists the fitted drainage parameters along with other soil parameters required for the numerical simulations.

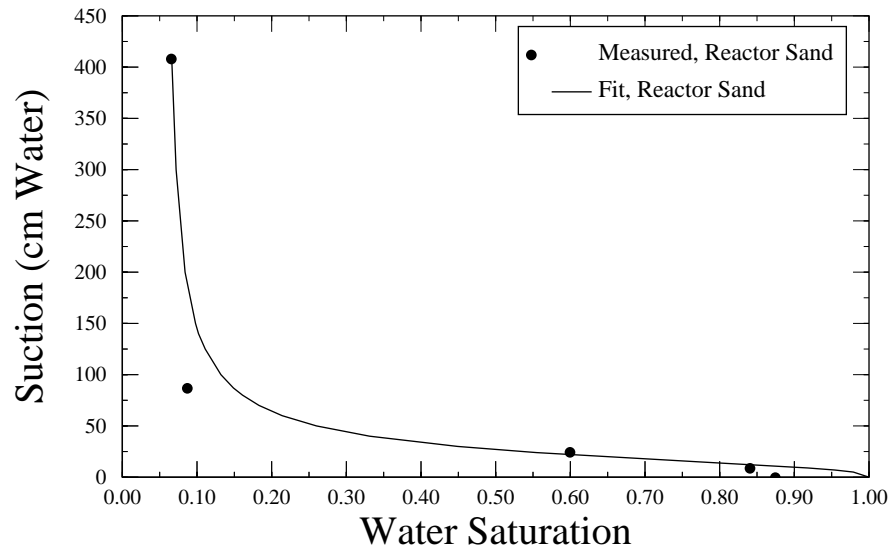


Figure 9: Drying Characteristics of Sand Measured under Drainage Cycle (Data Measured by Daniel B. Associates, Albuquerque, NM; Fitted Van Genuchten Curve (line) Was Obtained Using a Program Developed by Parker, et al. (1987))

Table 3: Porous Media Properties For T2VOC Simulations

Property	Value
Porosity	0.25
Bulk Density	2.0 g/cm^3
Absolute Permeability	1.0 $\times 10^{-10} \text{ m}^2$
α	5.4 m^{-1}

Property	Value
n	2.5
S _{wr}	0.06
N	3

In conjunction with air saturation, gas permeability directly influences the stripping rate. Relative gas permeability is the ratio of the gas permeability at a given water saturation to the gas permeability for completely dry (or saturated) conditions (absolute permeability). For two-phase flow, the relative permeability is a function of the gas and residual water saturations. Equation (11) is used by T2VOC to calculate the relative gas permeability for a two-phase system.

$$k_{rg} = \left(\frac{S_g}{1 - S_{wr}} \right)^N \quad \text{for } 0 < S_g < 1 - S_{wr} \quad (3)$$

$$k_{rg} = 1 \text{ for } S_g \geq 1 - S_{wr}$$

where: k_{rg} =relative permeability, S_g =gas saturation ($1-S_w$), and N = empirical constant between 2 and 4.

Figure 10 is a plot of equation (3) assuming $S_{wr} = 0.06$ (taken from Figure 4) and $N=3$, which has been found to be applicable for unconsolidated sands (Faust et al., 1989). The two points on the graph denote measurements of relative gas permeability for the sand at two water saturations. The method for measuring the gas permeability at the two water saturations and the absolute permeability under dry conditions was analogous to a constant-head permeameter. The absolute permeability of the sand is 10^{-10} m^2 . The data shown in Figure 9 indicate that the $N = 3$ and $S_{wr} = 0.06$ assumptions were adequate for this sand in that the calculated values and the actual data match very well, at least for water saturations between 40 and 60%.

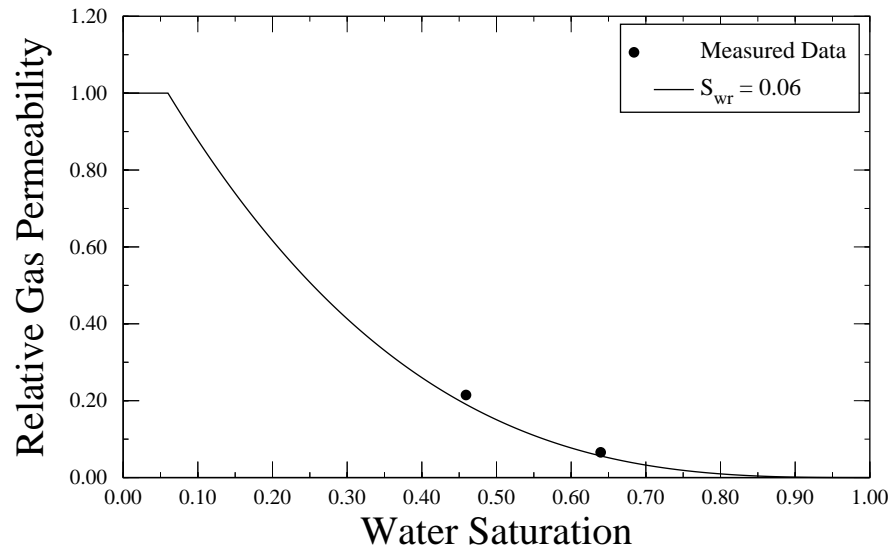


Figure 10: Water Saturation Versus Relative Gas Permeability

An axisymmetric grid was generated according to the following specifications: radial (column) discretization of 0.64 cm for the well, 2-cm widths out to 18 cm from the well, and then 4-cm widths out to edge of the reactor (60 cm); and a uniform vertical (row) discretization of 4 cm. A constant pressure (atmospheric) boundary condition was established at the top of the sand surface. The walls of the tank were no flow boundaries. The initial location of the water table and corresponding capillary fringe were generated with T2VOC for the initial conditions. The model was run until an apparent steady-state condition was achieved. Model-calculated air saturations and velocities were converted to fluxes so that a direct comparison to the measured fluxes could be made.

Preliminary Large-Scale Reactor Findings and Discussion

Although the laboratory tests were completed at several injection flow rates, only the 62, 187, and 283 LPM tests are reported. The data are presented in terms of air flux as a function of distance from the air sparge well (Table 4). Each experiment was analyzed first to determine if the measurements of flux represented the rate of air injection (flow balance). The four measured fluxes at a particular radial position were averaged arithmetically, and the averages for each radial position are listed in Table 6. The average was multiplied by the area of a ring 10-cm wide and centered at a distance equal to the radial distance of the center of the four measuring points (Figure 8) to obtain flow rates. The sum of the calculated flow rates through each concentric ring was compared to the measured injection rate to ascertain the flow balance of an experiment. The replicate high-flow (283 LPM) tests (Tests 1 and 2) exhibited a flow balance of 104 and 88 percent, respectively. The flow balances for the injection rates of 62 and 187 LPM were better than 98 percent each. The T2VOC predictions are compared to the average flux measurements for these experiments. Other experiments, not reported here, yielded similar trends and values of fluxes as those presented below, but for unknown reasons the discrepancy between the injection rate and the flux measurements was greater.

Table 4: Comparison of Measured Fluxes and T2VOC Predictions for Three Injection Rates.

Injection Rate (LPM):		62		187		283							
Radial Position of Flux Measurement Center (cm)	Radial Limits for Flow Calculation (cm)	Flow Flux (cm/s)		Flow Flux (cm/s)		Flow Flux (cm/s)				Percentage of Injection Flow Rate			
		Measured Average	T2VOC	Measured Average	T2VOC	Measured			T2VOC	Calculated from Measured			T2VOC
						Test 1	Test 2	Average		Test 1	Test 2	Average	
5	0-10	1.01	1.04	1.91	1.59	2.49	3.09	2.79	1.91	17	21	19	14
15	10-20	0.44	0.69	1.32	1.18	2.18	1.77	1.98	1.47	43	35	39	33
25	20-30	0.12	0.30	0.63	0.66	0.97	0.70	0.84	0.90	32	23	28	26
35	30-40	0.021	0.07	0.091	0.22	0.18	0.17	0.18	0.35	8	8	8	22
45	40-50	0.0002	0.005	0.001	0.033	0.053	0.009	0.031	0.071	3	0.13	2	4
55	50-60	0.00	0.0003	0.00	0.003	0.005	0.003	0.004	0.007	0.6	0.6	0.6	1

Preliminary Cylindrical Reactor Laboratory Results

The measurements of two replicate sparging tests completed at 283 LPM are shown in Figure 11. The averages of the measured fluxes are reported in Table 6. The largest differences between the two tests occur within the first three radial positions. Figure 10 illustrates that although the sand media was assumed to be homogeneous and isotropic and the average flux distributions were similar, the measured sparging patterns were not. In Test 1, the flux varied from approximately 2.0 to 3.6 cm/s at the first radial position. For both tests, the flux exiting the groundwater table is approximately zero at 45 cm from the injection well. The trend of high flow fluxes near the well that rapidly drop to zero with increasing radial distance was observed qualitatively in the field study by Leeson et al. (1995); where they observed as the distance from the well increased, the frequency of the bubbles appearing at a given location and the number of places that the bubbles exited the water surface decreased rapidly.

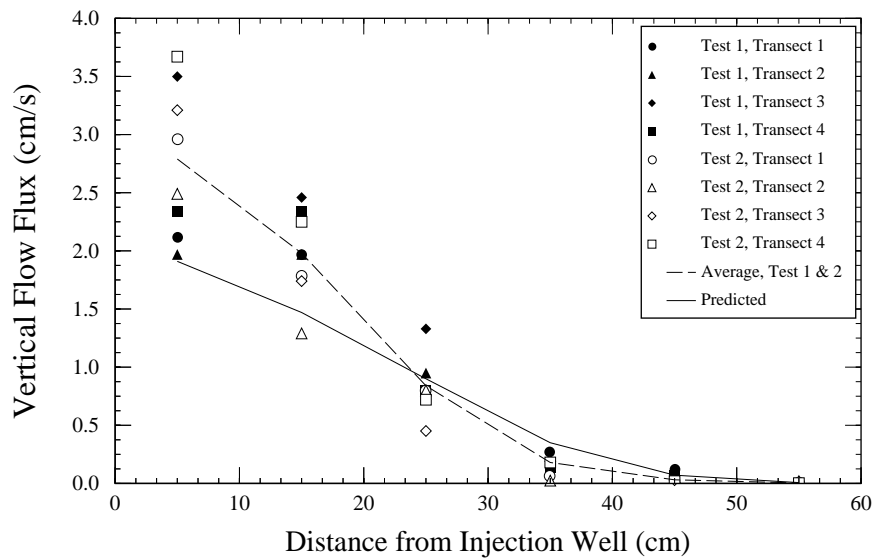


Figure 11: Measured and Predicted Vertical Fluxes in the Cylindrical Reactor for a 283 LPM Injection Rate

The average fluxes listed in Table 4 also illustrate the influence of the injection rate. Although the flow flux is greater at each radial point for an increased injection rate, the fractions of the total flow are similar. No flow was detected at the outer radial position for the 187 and 62 LPM injection rates, whereas flow was detected at the tank wall for the higher injection flow rate. For the three flow rates, 90 percent of the flow injected was exited within the first 3 radial positions. These observations are consistent with those from the numerical study by Lundegard and Andersen (1996).

For all the experiments, the measured flux values varied similar to that depicted in Figure 11. In addition, when measurements were repeated at a particular point, the rate would change with time. Therefore, the measurement procedure was standardized among the tests. This variability was also apparent in the sight gage, in which the water level would fluctuate continuously throughout the experiment. The frequency and amplitudes of the fluctuations would become constant for a given injection rate. Although piezometric levels in field monitoring of

sparging has been shown to change with time, never has it been reported that the levels would oscillate as we observed. We attribute the oscillatory effect to the influence of the reactor walls and, possibly, a dynamic nature of the sparging process where air channels may change with position even over extended periods. The experiments of Ji et al. (1993) did not show this phenomenon even though the conditions for several of their experiments were quite similar to the ones presented herein. The primary difference was their flow field was constrained to two dimensions.

Preliminary Simulations

Simulations with T2VOC were also completed for all the experiments, but only the 283 LPM results will be presented because the results are representative of the others. First, the averages of the flux measurements as a function of radial distance from the sparge well were analyzed. Next, analysis of the sparging regime in two dimensions is considered.

The predicted flow flux ranges from 0.007 cm/s at the reactor boundary to 1.91 cm/s adjacent to the injection well, which is less than the measured range of 0.006 cm/s to 2.79 cm/s. The simulation indicates that the air flux drops to approximately zero about 45 cm from the well which is also shown in the measured data. The laboratory system had a larger range of values due to localized heterogeneity (Ji et al., 1993), which caused the air to find other less restrictive pathways.

The fractions of total flow calculated from the data and the model are compared in Table 2. The predicted and measured values coincided for all radial positions although the specific flux values do not (Figure 11). In general, the second radial position showed the highest fraction of flow for all cases. The fractions of total flow at 283 LPM were also similar to the ones found in the other tests. Lundegard and Anderson (1993) observed that the sparging regime becomes constant after a test has run for a given period and that increases in injection rates were compensated primarily by higher fluxes in the near-well vicinity with very small incremental increases in the sparge regime volume. A constant sparging pattern also occurred in field-scale numerical experiments completed using T2VOC by McCray (1994). Our data are consistent with their observations.

The largest discrepancies between the data and model predictions are nearest the well (Figure 11). As the distance from the injection well increased, the flow flux and the difference between the predicted and measured values decreased. One reason for this may be due to the difference between the fit of the van Genuchten formula and the measured pressure-saturation data (Figure 9). The saturations nearest the well are in the range where the fit pressure-saturation curve and data have the greatest discrepancy.

To test if the reactor walls constrained the sparging pattern, an axisymmetric simulation was completed for the same groundwater table elevation, sparge well depth, and injection flow rate (283 LPM), but the simulated reactor diameter was increased to 2.0 m. For the 2.0-m diameter simulation, 93 percent of the injected air evolved from the groundwater table within 60 cm of the injection well, compared to 30 cm for the 1.2-m diameter simulation. The enlarged configuration predicted that approximately 50 percent of the injected flow exited within 30 cm of

the sparge well and 75 percent of the injected flow exited within 40 cm of the injection point. This result seems to imply that the sparging regime increased 10 cm by extending the reactor walls out to 2 m.

T2VOC Modeling Applications

From a design standpoint, the level of agreement between the reactor data and the multiphase-flow model, T2VOC, is probably acceptable. Therefore T2VOC may be used for describing general air flow patterns expected in a field situation where the soils are relatively homogeneous, isotropic, and permeable. The recommended procedures for data input consist of: (1) obtain accurate soil properties (porosity, pressure-saturation data, and absolute permeability), (2) measure at least one relative gas permeability to determine whether the permeability-saturation formulation is appropriate, and (3) select a system configuration consistent with conventional practices for the particular site (soil type, depth to groundwater, contaminant locations). Further testing of the multiphase flow models is needed before wide acceptance of a particular model is achieved. Vertical measurements of gas or water pressure, measurements at larger scales more representative of field conditions, heterogeneities, and influences of adjacent sparge wells are all issues still to be considered. Moreover, the three fluid phases (air, water, and NAPL) and chemical transport aspects of the models are yet to be tested.

Summary of Preliminary Experimental and Modeling Results

Preliminary experiments have also been completed in a cylindrical reactor under controlled conditions to measure and simulate the air flow distributions at the water table. A theoretically based multiphase flow model could simulate the radially averaged-flux distribution using independently measured parameters. Although the sparging model was able to predict the average flow flux distribution, it could not simulate the variability of the measured data due to the assumption of radial symmetry. As expected, the fluxes were greatest closest to the sparge well and decreased almost exponentially with distance from the sparge well. The results from these tests showed that the region of influence increases only slightly with an increasing injection flow rate, because the primary changes were increases in fluxes nearest the sparge well. As the injection flow rate increased, the flow flux nearest the well increased proportionally, whereas the region of influence enlarged only slightly. The modeling showed that the reactor configuration limited the sparging pattern. Therefore, when modeling an actual sparging system, the system boundaries should be configured such that their effect on the air flow pattern is consistent with what would occur in the field.

Application/Benefits

Since the primary goal of this project is to obtain a greater understanding of the mass transport mechanisms involved in air sparging, we plan to provide documentation to aid in the design and application of this technology by:

- Providing guidance for conducting laboratory tests of and developing mechanistically correct models for air sparging tests.

- Developing a field-scale air sparging model to obtain more effective treatment, more realistic estimates of remediation times and improved design configurations.
- Providing design guidance for air sparging that takes into consideration the impacts of mass transfer.

These deliverables will aid engineers and scientists, both in the field and laboratory, in the design and implementation of air sparging systems. They will also indicate which design parameters have the greatest impact on air sparging operation.

Future Activity

This project is composed of two sections: model development and laboratory experiments. These parts will be completed independently. Then model testing will be conducted using the laboratory data. The final model testing will be done by comparing numerical predictions to data obtained from a field site. When these tasks are finished, a users manual will be written such that engineers can use this code to predict the performance of an air sparging system at field sites and in the laboratory. The model development will be completed at Clemson University, while the laboratory testing and field data will be completed under the direction of Michigan Technological University.

Acknowledgments

We would like to thank the U.S Department of Energy for funding this research and Karl Frohne, the METC Contracting Officer's Representative for his guidance on this project. This research began in August 1996 and will be completed in two years.

References

Falta, R.W., K. Pruess, S. Finsterle, A. Battistelli, T2VOC User's Guide. Lawrence Berkley Laboratory, Report LBL-36400, March, 1995, pp. 1-155.

Gierke, J.S., N.J. Hutzler, and J.C. Crittenden, "Modeling the Transport of Volatile Organic Chemicals in Unsaturated Soils," WRR, Vol. 26, No.7, pp.1529-1547, 1990.

Gierke, J.S., N.J. Hutzler, D.B. McKenzie, "Vapor Transport in Unsaturated Soil Columns: Implications for Vapor Extraction". WRR, Vol. 28, No. 2, 1992, pp. 323-335.

Hein, G.L., N.J. Hutzler, J.S. Gierke, "Quantification of the Mechanisms Controlling the Removal Rate of Volatile Contaminants by Air Sparging", Proceedings of the 1994 National Conference on Environmental Engineering on Critical Issues in Water and Wastewater Treatment, ASCE, Environmental Engineering Div., Boulder, CO, July 11-13, 1994.

Hokanson, D.R., Development of Software Design Tools for Physical Property Estimation, Aeration, and Adsorption. MS Thesis, Michigan Technological University, 1996.

Ji, W., A. Dahmani, D.P. Ahlfeld, J.D. Lin, E. Hill, III, "Laboratory Study of Air Sparging: Air Flow Visualization". GWMR, Fall, 1993, pp. 115-126.

Johnstone, T.L., Modeling Solute Transport Under Fingered Flow Conditions: A Two-Dimensional Approach. MS Thesis, Michigan Technological University, 1995.

McCray, J.E., Numerical Analysis of Air Sparging for Subsurface Remediation. Masters Thesis, Clemson University, 1994.

Microsensor Technology, Inc., EZ Chrom 20 Chromatograph Data System, Operators Manual. P/N 20049, 1990.

Microsensor Technology, Inc., M200 Operations Manual. P/N 20050, 1990.

Millington R.J., J.P. Quirk, "Permeability of Porous Solids". Trans. Faraday Soc., Vol. 57, pp. 1200-1207.

Wojick, C.L., Transport of Solutes through Unsaturated Sand: Laboratory Experiments. MS Thesis, Michigan Technological University, 1995.